ACTA CHEMICA IASI, **34_1**, 229-256 (2026)
DOI: 10.47743/achi-2026-1-0010

Article

STUDIES OF VACUUM-ANNEALED SINGLE-LAYERED AND DOUBLE-LAYERED TiO_2 NANOCRYSTALLINE FILMS SENSITIZED WITH NATURAL DYES FOR DYE-SENSITIZED SOLAR CELL APPLICATIONS

Namita Singh, Sahiba Siddiqui and Namrata Ghildiyal*

Department of Chemistry, School of Sciences, Hemvati Nandan Bahuguna Garhwal University, Srinagar-Garhwal, Uttarakhand, India-246174

Abstract: In the present study, dye-sensitized solar cells (DSSCs) were constructed with photoanodes made from vacuum-annealed single- and double-layered nanocrystalline TiO_2 films sensitized with pigments present in the extract of bayberry fruit. A double layered titania film under normal air pressure was also prepared and tested for light harvesting efficiency in natural dye-based DSSC. The extract was analysed using high resolution-liquid chromatography mass spectrometry (HR-LCMS), UV-visible, Fourier transform infrared spectroscopy (FTIR) and nuclear magnetic resonance spectroscopy (NMR). The interaction of dyes with TiO_2 was studied by mid-IR and far-IR spectroscopy. The TiO_2 thin film surface was characterized by X-ray diffraction (XRD), scanning electron microscopy (SEM), energy-dispersive X-ray spectroscopy (EDX), X-ray photoelectron spectroscopy (XPS) and non-contact atomic force microscopy (nc-AFM). Vacuum annealing increases oxygen vacancies and Ti^{3+} defects in titania. The Ti^{3+} defects in the TiO_2 film were captured in the XPS spectra. The DSSC constructed from a 9-11 µm thick vacuum-annealed single-layered TiO_2 thin film photoanode displayed better performance (V_{OC} = 291 mV, I_{SC} = 0.591 mA, FF = 57 % and η = 0.32 %) than that built from double-layered vacuum-annealed titania film. Both had better efficiency than the one fabricated from conventionally annealed double-layered titania film. The results show that vacuum-annealing could

* Namrata Ghildiyal, *e-mail:* namoo_doon@yahoo.co.in

be an interesting field of study to explore the performance of natural dye-based DSSCs. The work also demonstrated the effect of thickness of titania film on performance of DSSC.

***Keywords*:** DSSCs, TiO_2; Nanocrystalline; Vacuum-annealed; Natural dyes

Introduction

Renewable sources are essential for a sustainable future because they are primarily clean, inexhaustible and can be harnessed locally.[1-3] This category includes energy from biomass, hydropower, geothermal heat, wind and solar energy. Among these, solar energy harvesting plays a crucial role in the conservation and sustainable use of energy. In 1991, *B. O'Regan* and M. Grätzel, invented the dye-sensitized solar cells (DSSC), also known as the Grätzel cell, which convert sunlight into electricity.[4] A dye-sensitized solar cell (DSSC) is a photoelectrochemical cell, which consists of a photoanode made of a nanocrystalline semiconductor oxide film, like TiO_2 film, deposited on a transparent conducting glass substrate (FTO/ITO), an electrolyte, photosensitizer (dye) and a counter electrode. Nanocrystalline TiO_2-based DSSCs employing natural dye as photosensitizers have gained attention as sustainable photovoltaic cells due to their low-cost, eco-friendly nature and potential for light-harvesting solar energy conversion efficiency.[5] Several pigments including anthocyanin, chlorophyll and betalains found in plant extracts have been evaluated for their light harvesting properties.[6-10] Each pigment has a distinct maximum absorption peak (λ_{max}) within the solar spectrum which is responsible for DSSCs electrical performance.[11] The word anthocyanins derived from a Greek word "Anthos" (flower) and "kiano" (blue). Anthocyanins belong to the polyphenolic class of compound also known as flavonoids that give plants their vibrant colours like red, purple and blue. The wild Himalayan bayberry (*Myrica esculenta)* is a tree with traditional medicinal uses that grows in subtropical forests in the Indian Himalayan and Indo-Malaya region at high altitudes. The Himalayan bayberry

shrub is popular in the native people of Uttarakhand due to its sweet taste and processed products like squash, jams etc. In addition, the Himalayan bayberry fruit also has anticancer and antioxidant properties. Its fruits are a rich source of pigments like anthocyanins that can act as photosensitizers in DSSCs.[12] Utilizing natural dyes such as chlorophyll, anthocyanin, carotenoid and flavonoid as photosensitizers in photoanode of TiO_2-based DSSCs has been a field of constant experimentation.[13] Titania nanopillars have achieved an efficiency of 0.46 % using photosensitizers derived from Pomegranate.[14] Blackberry extracts have displayed a PCE of 0.191 %, with 380 nm as optimum TiO_2 thickness using spin coating method.[15] Extract of Black plum (*Syzygium cumini*) fruits have served as a source of photosensitiser for DSSCs. Efficiency of these optimized DSSCs with a series of electrolytes was tested to extract a maximum efficiency of 0.205 %.[16] Jabuticaba fruit were coated on TiO_2 film. The efficiency and fill factor of the DSSC using jabuticaba fruit dye were 0.13 % and 0.29 %, respectively.[17] The results show that conversion efficiencies obtained from different plant extracts vary with concentration of the photosensitizer in the plant part, TiO_2 film parameters and annealing conditions. Studies on natural dye based DSSCs mainly focus on tuning these parameters to achieve better conversion efficiencies. Various approaches including blending different natural dyes, copigmentation of dyes and acidifying of dyes have been adopted to improve the efficiency of natural dye-based DSSCs.[18,19] Parameters that have been changed to enhance performance include film thickness, porosity, nanoparticle size and different deposition layers of titania.[20-25]

Titania nanocrystalline materials have been synthesized by various methods including sol-gel method.[26-27] The nanocrystalline powder so obtained was then deposited on conductive glass substrate and subjected to annealing conditions to obtain TiO_2 nanostructured thin films.

In the present work we have attempted to increase the defect states in TiO_2 films by vacuum annealing them under 70 torr at 500^oC for 1 hour.

Vacuum-annealing of TiO_2 films is known to increase defects such as oxygen vacancies and Ti^{3+} states.[28-30]

Surface defects introduce additional shallow energy states under the conduction band of TiO_2. This narrows the band gap and facilitates electron transport across dye-TiO_2 interface via the defect states. If the recombination of trapped electrons with the hole in ground state of the dye or with the electrolyte mediator does not exceed the electron injection rate into the TiO_2, the conversion efficiency of the DSSC can be improved.[31-33] Investigations on various utilities of extracts of *Myrica esculenta* have been reported in literature.[34-38] However, minimal studies have been conducted on photosensitizer properties of extract of *Myrica esculenta* for DSSC applications.[39]

In the present work we have investigated the conversion efficiency of DSSCs based on vacuum-annealed single- and double-layer TiO_2 nanocrystalline thin films that were sensitised with flavonoids present in the extract of Himalayan bayberry (*Myrica esculenta).*

Results and Discussion

HR-LCMS analysis

The HR-LCMS method was used for the identification and profiling of the metabolites present in the bayberry fruit extract.[40-46] Based on their retention time (RT), the HR-LCMS results of bayberry extract in acidified methanol showed a rich profile of phenolic and flavonoid compounds in both positive and negative ESI modes. Precise m/z values are reported in Table 1 and their chromatograms (both positive ESI mode and negative ESI mode) are shown in Supplementary Material, Figure S1 and structures of these compounds are shown in Supplementary Material, Figure S2. In positive ionization mode, the spectra showed polyphenolic compounds such as p-coumaric acid and malvidin-3-O-(6-O-acetyl-beta-D-glucoside indicating the presence of polyhydroxylated

aromatic systems and sugar conjugates. In negative mode, confirmation was obtained for additional phenolic constituents like gallic acid, catechin, luteoforol, epicatechin-3'-O-glucuronide and kaempferol-7-O-glucoside.

Table 1. Compounds identified in the HR-LCMS of bayberry extract in acidified methanol.

Bayberry extract							
Positive mode				Negative mode			
Compound name	Chemical Formula	R_T	m/z value	Compound name	Chemical Formula	R_T	m/z value
p-Coumaric acid	$C_9H_8O_3$	1.642	165.0532	Catechin	$C_{15}H_{14}O_6$	7.958	289.0716
				Luteoforol	$C_{15}H_{14}O_6$	7.918	289.0701
Malvidin-3-O-(6-O-acetyl-beta-D-glucoside	$C_{25}H_{27}O_{13}$	1.384	536.1543	Gallic acid	$C_7H_6O_5$	20.77	169.016
				Epicatechin-3'-O-glucuronide	$C_{21}H_{22}O_{12}$	4.657	465.1082
				Kaempferol-7-O-glucoside	$C_{21}H_{20}O_{11}$	4.676	447.0973

UV-visible spectroscopy

The UV-visible spectrum of the extract contains absorptions from a number of molecules present in the extract which leads to overlapping of peaks. Derivative of flavonol like kaempferol gave rise to two major absorption peaks in the region 240 – 280 nm (Band II) associated with absorption due to the A-ring and in the region 300 – 380 nm (Band I) attributed to absorption due to the B-ring. The UV-visible spectrum of bayberry extract showed an absorption maxima (λ_{max}) in the range 520 – 560 nm which is characteristic absorption peak of anthocyanins.[47]

Additionally, a broad absorption band at 400-450 nm was also recorded, which was attributed to sugar moieties connected to the anthocyanidin moiety as shown in Figure 1(a).[48] The total anthocyanin content in the extract was determined using reported method and was found to be 32.514 mg/L for cyanidin-3-O-glucoside and 33.091 mg/L for malvidin 3-O-(6-O-acetyl-beta-D-glucoside).[49] The absorption edge of titania (400 nm) was obtained from UV-visible spectra of titania film and dye-sensitized titania film as presented in

Figure 1(b). The analysis of the spectra showed that the maximum absorption of titania at 320 nm undergoes a minor bathochromic shift to 328 nm after sensitization with the dyes present in the extract. The UV-visible spectra of the sensitized titania layer showed the presence of flavonoids with absorption maxima, λ_{max}, at 540 nm. Spectral variations were observed in the UV-visible spectrum as the pH varied from 1 to 4.5 indicating structural changes in the flavonoid molecules.

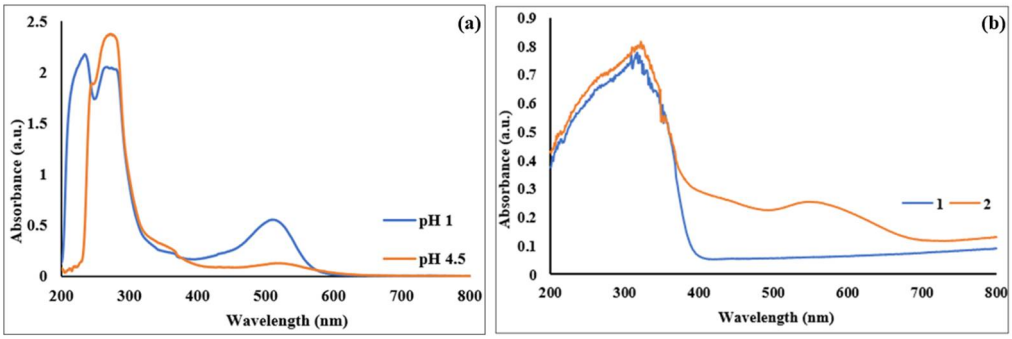

Figure 1. The UV-visible spectra of **(a)** Bayberry extract in pH 1 and pH 4.5 **(b)** normal titania film (1) and titania film stained with bayberry extract (2).

FTIR analysis

The FTIR spectrum, Figure 2(a), shows the transmittance of ambient pressure annealed and vacuum-annealed titania powder. Both nano powders exhibited nearly intense broad absorptions in the 900-400 cm^{-1} region corresponding to Ti-O and O-Ti-O stretching vibrations in various surface states. The strong band observed at 456 cm^{-1} was assigned to Ti-O-Ti stretching vibration in nanocrystalline anatase particles. Minimal moisture on TiO_2 surface was indicated in the O-H stretching vibration region (3200 – 3550 cm^{-1}) of the spectrum showing that the surface was free for dye adsorption. The FTIR spectrum of the bayberry extract and TiO_2 thin film sensitized with the bayberry extract given in Figure 2(b) showed many characteristic bands of flavonoids. The mid-IR spectrum of bayberry extract had a broad O-H stretching band

mainly from phenolic hydroxyl group stretching with maximum at 3379 cm^{-1} that narrows and shifts to 3408 cm^{-1} in the dye-stained TiO_2 confirming interaction between the TiO_2 and hydroxyl groups of phenolic compounds.[50] Wide O-H bonds were indicative of presence of carboxylic acids like coumaric acid that is one of the components present in the extract. The bands at 2933 and 2898 cm^{-1} were attributed to C-H stretching vibrations in molecules like catechin and anthocyanin. The peak at 1726 cm^{-1} was assigned to C=O stretching vibration of aromatic esters and -COOH groups. The ring C=C stretching vibration of all types of flavonoids fell in the region 1650–1560 cm^{-1}. Medium intensity bands at 1410 and 1334 cm^{-1} were assigned to C-H bending vibrations. The bands observed between 1300-1000 cm^{-1} were attributed to C-O-C and C-O-H stretching of glycosidic moieties confirming the interaction of sugar moieties with TiO_2 nanocrystalline film.[51] Strong bands at 1242 cm^{-1} were attributed to C-OH deformation vibrations. The ring vibration of anthocyanin was observed at 818 cm^{-1}. A comparison of the mid-IR spectra of the extract and dye-stained TiO_2 nanocrystalline sample showed that many intense peaks, characteristic of the dyes present in the extract, reduced in intensity after adsorption on the TiO_2 nanocrystalline film surface. Spectral changes were observed after dye adsorption in regions ranging from 1731 to 1637 cm^{-1}, 1367 to 1228 cm^{-1} and 680 to 592 cm^{-1} in the mid-IR, Figure 2 (b). This may be due to removal of other molecules present in the extract from the surface of TiO_2 after adsorption process. The Ti-O-Ti stretching peaks also disappeared showing some obstruction to this vibration on dye adsorption. The far-IR spectrum Figure 3(a) was replete with Ti-O and Ti-O-Ti lattice vibrations. The region above 300 cm^{-1} in far-IR spectrum of dye-stained TiO_2 Figure 3(b) showed additional peaks from interactions due to organic molecules present on TiO_2 surface.

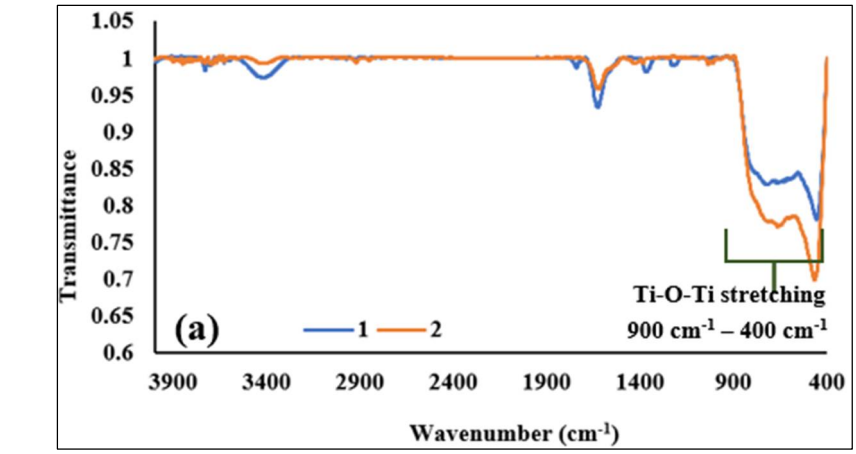

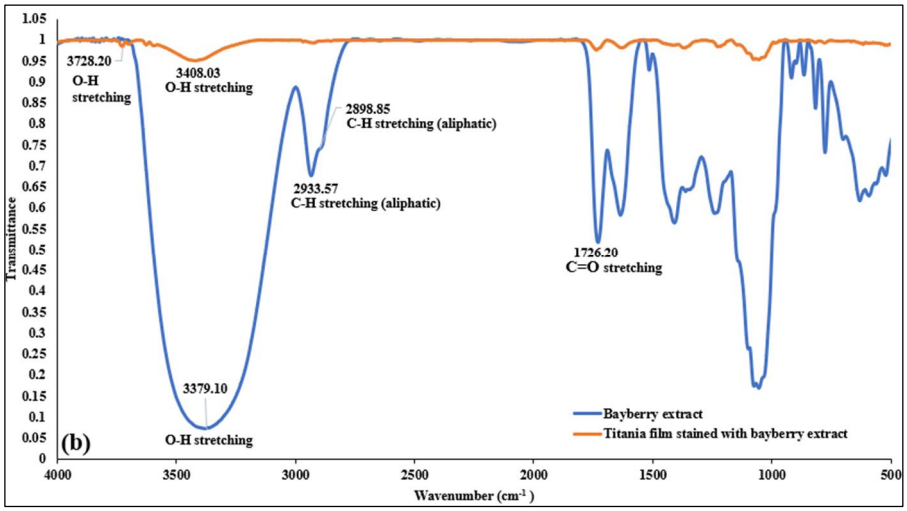

Figure 2. Mid-IR spectrum of: **(a)** nanocrystalline titania nano powder annealed at normal pressure conditions (1) and annealed in vacuum at 500°C (2); **(b)** bayberry extract and bayberry extract stained nanocrystalline TiO_2 annealed under ambient pressure conditions at 500°C.

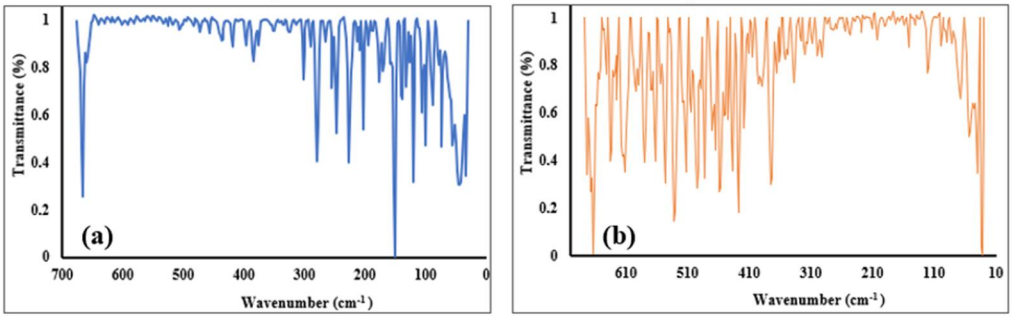

Figure 3. **(a)** Far-IR spectrum of the nanocrystalline titania nano powder annealed at normal pressure conditions; **(b)** Far-IR spectrum of TiO_2 surface prepared by annealing under ambient pressure conditions at 500 °C and stained with the bayberry extract.

NMR analysis

The NMR signals were largely overlapping due to the close structural similarity of anthocyanins and the complexity presented by the composition of the extract. The ^{1}H NMR spectrum of bayberry extract in methanol-d_4 presented in Figure 5 showed some of the characteristic peaks that support the presence of anthocyanin derivatives in the extract. Chemical structures and numbering of atoms of cyanindin-3-O-glucoside and malvidin 3-O-(6-O-acetyl-beta-Dglucoside) are shown in Figure 4.

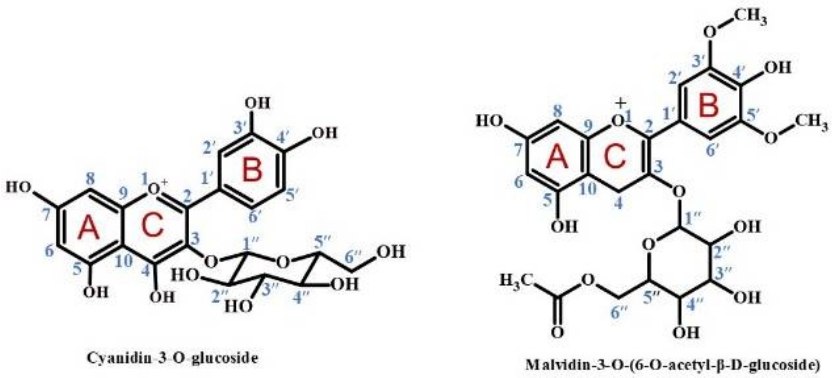

Figure 4. Chemical structure of cyanindin-3-O-glucoside and malvidin 3-O-(6-O-acetyl-β-D-glucoside).

The ^{1}H NMR spectrum in DMSO-d_6, ^{13}C NMR spectrum in methanol-d_4 and ^{1}H-^{13}C HSQC spectrum in DMSO-d_6 spectra of bayberry extract are presented in Supplementary Material, Figure S3, Figure S4 (a)-(c) and Figure S5, respectively. The resonance signals for protons H-6, H-2″, H-3″, H-4″/ H-5″and H-6″ of cyanindin-3-O-glucoside appeared at 6.8, 3.5, 3.4, 3.2, 3.4 and 3.7 ppm, respectively, in methanol-d_4. The ^{13}C NMR chemical shifts for C-6, C-2″, C-3″, C-4″ and C-5″ were observed at 102.8, 73.2, 76.1, 69.0 and 77.5 ppm, repectively, in methanol-d_4.

The ^{1}H and ^{13}C NMR data in methanol-d_4 was analyzed for malvidin-3-O-(6-O-acetyl-β-D-glucoside). The molecule is characterized by its

anthocyanidin core, sugar moiety and acetyl group.[52] The ^{1}H NMR chemical shifts corresponding to H-6 and H-8 were observed at 6.80 and 6.95 ppm, respectively. The signals for H-6"a, H-6"b were observed in the range δ 4.40 – 4.50 ppm. The -OCH_3 (at H-3' and H-5') was observed at δ 4.05. The signal for anomeric proton (β configuration) was observed at 5.20 ppm. The acetyl group protons were observed at 2.05 ppm. The carbon resonances at 105.6, 93.5, 74.4, 73.5, 71.2 ppm in the ^{13}C NMR spectrum of the extract in methanol-d_4 were assigned to C-6/C-1″, C-8, C-5″/C-2″, C-3″ and C-4″, respectively. The ^{1}H-^{13}C HSQC spectra was highly crowded for cross peak assignment.

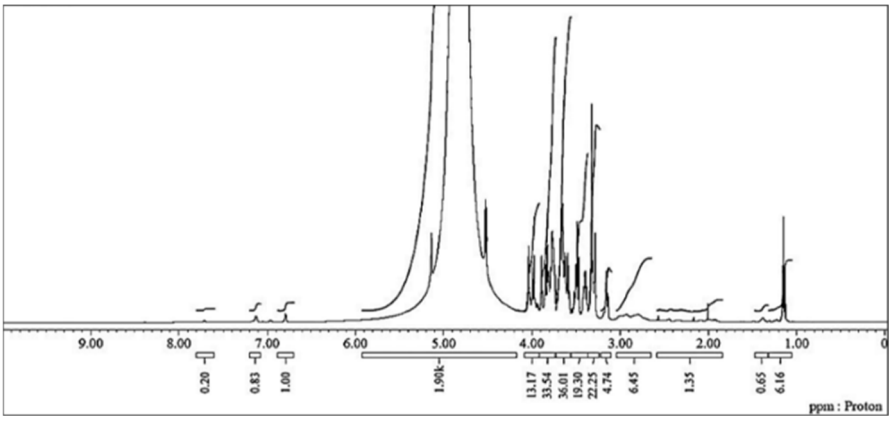

Figure 5. ^{1}H NMR 600 MHz of bayberry extract in methanol-d_4.

XRD analysis

The phase of TiO_2 affects the extent of dye adsorption and hence the performance of a DSSC based on natural dyes. Anatase phase exhibits best organic dye adsorption amongst the three polymorphic forms of TiO_2 viz. anatase, rutile and brookite. The XRD patterns of TiO_2 nano powder prepared by sol-gel method exhibited diffraction peaks at 25.2°, 37.8°, 48.03°, 53.9° and 62.6° indicating presence of nanocrystalline TiO_2 in the anatase phase, as shown in Figure 6(a). The Scherrer formula, $d = (0.9 \lambda / \beta \cos\theta)$ was used to calculate the average crystallite size (d) of TiO_2 nanoparticles at most intense peak (101)

plane where λ is X-ray wavelength of 0.15406 nm, β is full width half maxima and θ is the Bragg's diffraction angle.[53,54] The average particle diameter of TiO_2 nanoparticles was found to be 9.1 nm.

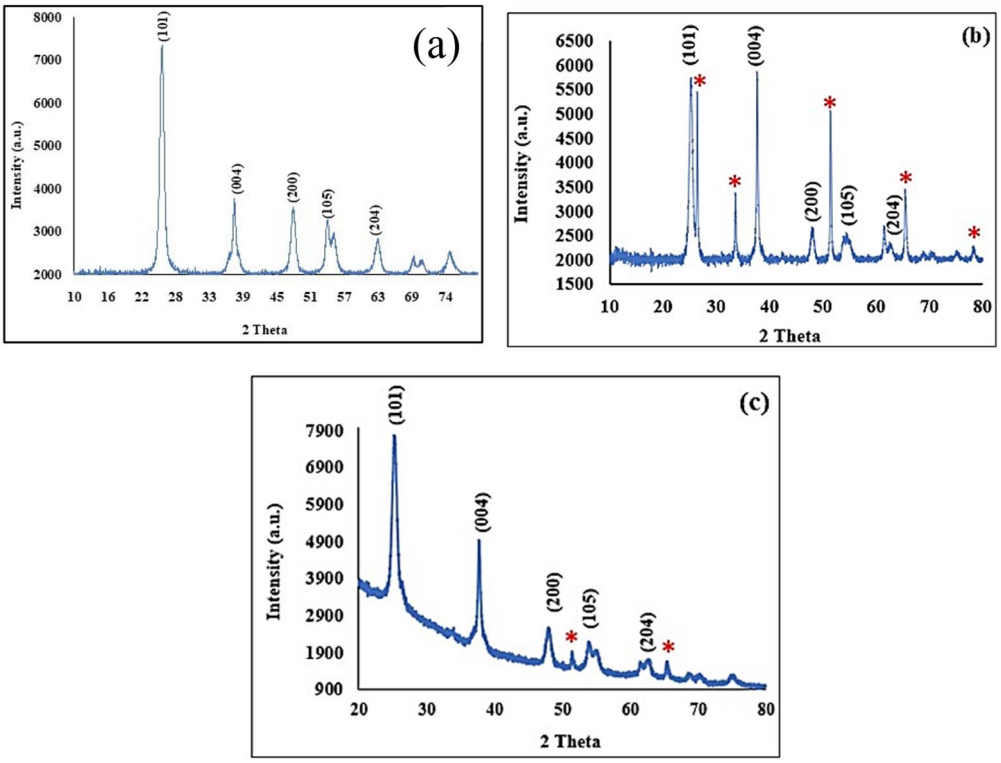

Figure 6. XRD pattern of **(a)** TiO_2 nano-powder (anatase phase); **(b)** TiO_2 thin film (**SLVA**) annealed at 500° C in vacuum for 1 hour (anatase phase); **(c)** TiO_2 thin film (**DLA**) (anatase phase).

The sample from TiO_2 thin film annealed in vacuum (**SLVA**) showed anatase phase in its XRD spectra with diffraction peaks at orientation planes of (101), (004), (200), (105), (204) at 25.2°, 37.6°, 48.0°, 53.9° and 62.3° as shown in Figure 6(b). The XRD patterns were indexed for anatase form of titania and matched well with the data of *JCPD card* No. 21-1272.[55,56] The average crystallite size of TiO_2 nanoparticles at most intense peak (101) plane, using Scherrer formula was found to be 10.4 nm. The SnO_2 peaks on FTO substrate

were detected at the orientation planes of (110), (101), (200), (211), (301), and (321), corresponding to angles of 26.4, 33.6, 51.4, 65.4 and 78.3°, respectively and marked using asterisk (*) in the Figure 6(b). These matched with the International Centre for Diffraction Data, ICSD (98-003-9177). The XRD peaks of annealed TiO_2 film **DLA** were observed at orientation planes (101), (004), (200), (105), (204) at 25.2°, 37.6°, 48.0°, 53.9° and 62.3° 2θ values confirming anatase phase, Figure 6(c).

SEM and EDX analysis

The SEM images, Figure 7(a) and (b), illustrate the top-view and cross-sectional features of the **SLVA**, respectively. The SEM image of the TiO_2 thin film deposited over FTO glass slide showed a highly porous and densely packed nanostructured surface. However, some agglomeration was also noticed. The size of the TiO_2 nanoparticles marked in Figure 7(a) fell in the range of 16.58 – 26.95 nm showing that a good working size of TiO_2 nanoparticles was achieved in the present work. The rough and irregular surface morphology of the layer provided a large surface area for effective dye adsorption leading to enhanced light-harvesting.[57] The cross-sectional image of the same single-layer TiO_2 thin film, Figure 7(b), showed a film thickness in the range of 9 – 11 μm. The SEM image of **DLVA** depicting morphology and structural features showed the size of particles was in the range of 9-17 nm and are marked in Figure 7(c). The film thickness of the **DLVA** (45.07 μm) is shown in Supplementary Material, Figure S6(a). The difference in film thickness of **SLVA** and **DLVA** explains the better photovoltaic performance of the single-layered TiO_2 film (**SLVA**). The EDX spectrum of the double-layered TiO_2 thin film annealed at 500° C in vacuum (**DLVA**), is shown in Figure 7(d). The SEM analysis of **DLA** showed the

surface of titania film with a rough and porous granular morphology and the cross-sectional image depicted a film thickness of about 73 µm, Supplementary Material, Figure S6(b) and (c). The EDX spectrum and elemental mapping, Supplementary Material, Figure S6(d) of the film shows titanium and oxygen as the component elements of the film. The EDX analysis showed the quantitative elemental composition of the prepared thin film of TiO_2. The EDX mapping elemental data is given in Table 2. It shows lower oxygen to titanium atomic % ratio in **DLVA** as compared to **DLA**.

Table 2. EDX elemental detection of the prepared thin film of TiO_2.

Element	DLA		DLVA	
	Weight %	Atomic %	Weight %	Atomic %
O K	49.05	74.24	45.1	71.1
Ti K	50.95	25.76	54.9	28.9

Non-contact AFM analysis

Non-contact AFM technique was used to characterize surface roughness and topography of the TiO_2 nanocrystalline films (**SLVA** and **DLVA**) vacuum-annealed at 70 torr for 500 °C, Supplementary Material, Figure S7 (a) to (d). The root mean square parameter (*Rq*) for normal TiO_2 thin film was 20.23 nm and dye-stained TiO_2 nanocrystalline thin film was 48.80 nm.[58]

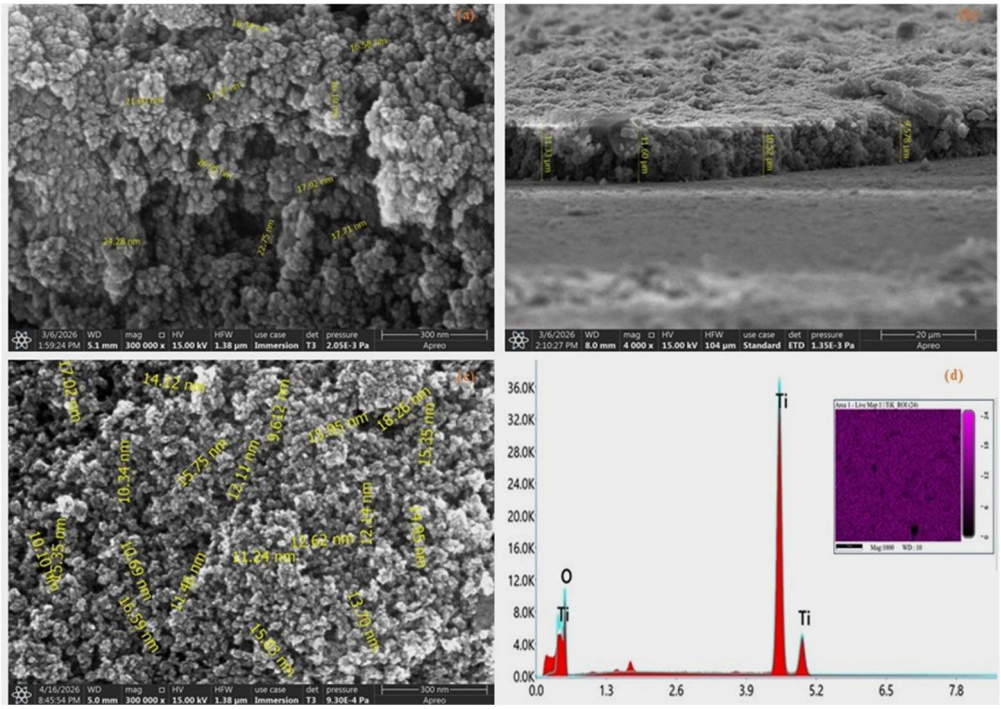

Figure 7. (a) SEM image of surface morphology of **SLVA** (b) cross-sectional micrographs of **SLVA** (c) **DLVA** surface morphology image (d) EDX spectra and mapping of **DLVA.**

XPS analysis

The XPS analysis showed that the major elements present in the thin film, **SLVA**, were titanium and oxygen, Figure 8 (a)-(c). The asymmetry of Ti 2p peaks indicated that apart from Ti^{4+} some other titanium species may also be present. Oxygen vacancies (V_o) cause reduction of Ti^{4+} to Ti^{3+} and increase the Ti_2O_3 content in the sample. This high-resolution Ti 2p spectra showed that Ti^{4+} $2p_{3/2}$ peak at 458.6 eV masked the Ti^{3+} $2p_{3/2}$ peak which has a binding energy of 457 eV, Figure 8 (b). The peak at 464.1 eV corresponds to the Ti^{4+} $2p_{1/2}$ which shows overlapping with Ti^{3+} $2p_{1/2}$ defect state peak which has a binding energy of 462 eV in the TiO_2 film. The peak at 528.0 eV was attributed to O (1s), while the residual C 1s peak appeared at 284.0 eV.[59] The auger peaks for Ti (Ti_{LMM})

and O (O_{KLL}) were present at 1070 and 970 eV, respectively. The Ti 2s, and Ti 3s and Ti 3p were observed at 563.5, 61 and 35.5 eV, respectively.

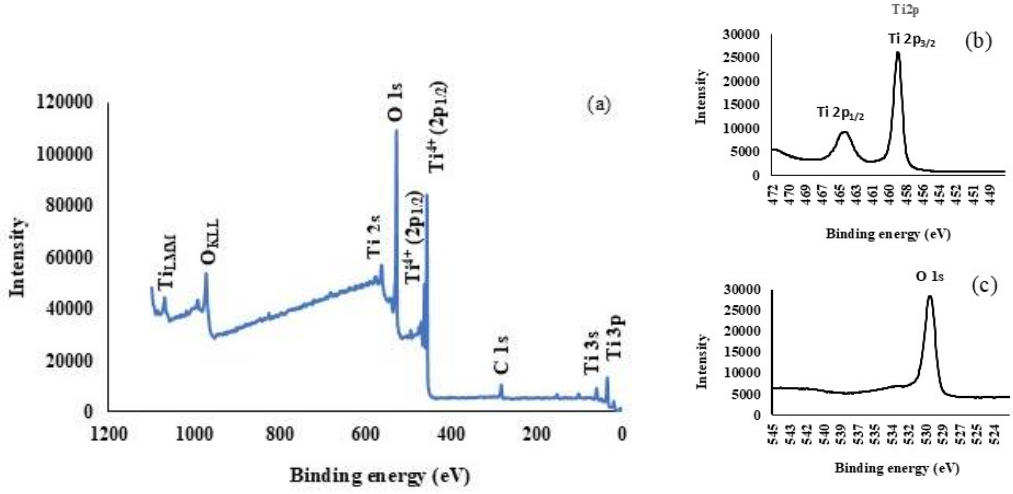

Figure 8. XPS of **SLVA:** (a) survey spectrum; (b) high-resolution Ti2p; (c**)** high-resolution O1s.

Solar simulator

The performance of fabricated DSSCs was evaluated from the *I-V* curves as shown in Figure 9.

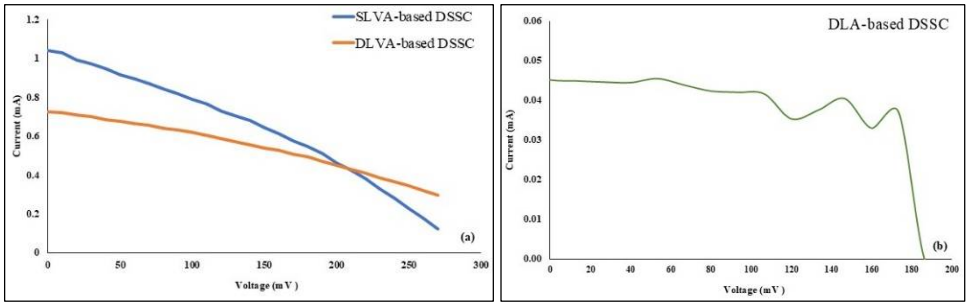

Figure 9. *I-V* curve of: **(a)** SLVA-based and DLVA-based DSSC; **(b)** DLA-based DSSC.

A comparison of performance of DSSCs prepared from all three methods showed that SLVA-based DSSC exhibited the best conversion efficiency. The photovoltaic characterization of the SLVA-based DSSC showed an open-circuit voltage (V_{OC}) of 291 mV and a short-circuit current (I_{SC}) of 0.591 mA. The device had a fill factor (*FF*) of 57 %, resulting in an overall power conversion

efficiency (η) of 0.32 %. The DLVA-based DSSC gave an open-circuit voltage (V_{OC}) 362 mV, with a short-circuit current (I_{SC}) of 0.725 mA, a fill factor (*FF*) of 34 % and efficiency (η) of 0.09 %. The fabricated DLA-based DSSC device exhibited an open-circuit voltage (V_{OC}) of 186 mV with a short-circuit current (I_{SC}) of 0.045 mA, a fill factor (*FF*) of 76 %, with an efficiency (η) of 0.06 %. The wavy I-V curve for DLA could be a consequence of energy level mismatches, high interfacial resistance or charge trapping and accumulation. Vacuum-annealing titania thin films results in sites that cause stronger coupling of energy states of the excited dye molecules with the conduction band via underlyimg shallow defect states of TiO_2 semiconductor film which improves electron injection rates in the dye-TiO_2 interface. This leads to improved performance of the DSSC. The photovoltaic performance of all the three devices is summarized in Table 3.

Table 3. A comparative study of the solar testing of SLVA, DLVA and DLA-based DSSCs.

Parameter	SLVA-based DSSC	DLVA-based DSSC	DLA-based DSSC
V_{oc} (mV)	291	362	186
I_{sc} (mA)	0.591	0.725	0.045
FF (%)	57	34	76
η (%)	0.32	0.09	0.06

Experimental

Materials for constructing a DSSC

Fluorine-doped tin oxide (FTO) conductive glass plates with sheet resistance of 7 Ω/cm^2 with the dimensions L 25 mm × W 25 mm × T 2.2 mm were purchased from Techinstro. Acetic acid (99 %), potassium iodide (99.8 %) and acetonitrile (99.8 %) were purchased from Merck. Titanium tetraisopropoxide (TTIP) (97 %), poly-L-Lysine (PLL) (98 %) and chloroplatinic acid hexahydrate solution was bought from Sigma-Aldrich.

Ethanol (99.9 %) and alpha-terpineol (95.09 %) were purchased from Tokyo Chemical Industry (TCI). Ethyl cellulose powder (98 %) and methanol (94 %) were procured from Central Drug House (CDH). De-ionized water was bought from Oscar Medicare Pvt. Ltd. The fruits of bayberries (*Myrica esculenta)* were collected from the terrace fields of Khirsu village, located in the district of Pauri Garhwal, Uttarakhand, India.

Instrumentation used for characterization of bayberry extract, TiO_2 nano powder, TiO_2 nanocrystalline thin film and solar simulator studies

The bayberry extract, TiO_2 nano powder and nanocrystalline thin-film were characterized using a number of analytical techniques. UV-visible absorption spectra were recorded using Lambda 25 UV-Vis Spectrometer (Perkin Elmer) and Cary 100 UV-Vis Spectrophotometer (Agilent Technologies). Fourier transform infrared (FTIR) spectra were obtained using a 3000 Hyperion Microscope coupled with a Vertex 80 FTIR System (Bruker, Germany). Structural characterization of bayberry extract was performed using an ECZR Series 600 MHz NMR spectrometer (JEOL, Japan) for ^{1}H, ^{13}C and HSQC analyses and a Q-Exactive Plus Biopharma mass spectrometer (Thermo Scientific, USA) coupled with a quaternary UHPLC system for HR-LCMS measurements. The nanocrystalline structure of TiO_2 samples was analyzed by X-ray diffraction (XRD) using a PANalytical Empyrean diffractometer with Cu $K\alpha$ radiation ($\lambda = 1.5406$ Å) over a 2θ range of 20°-80°. Surface morphology and elemental composition were examined using Sigma 300 scanning electron microscope equipped with EDX (Carl Zeiss). Surface topography was investigated using a Park Systems NX10 atomic force microscope (AFM) with PPP-NCHR cantilever. X-ray photoelectron spectroscopy (XPS) measurements were performed using a PHI 5000 VersaProbe III system. The photovoltaic performance of the fabricated DSSCs were recorded on a solar simulator of AM 1.5G, Class AAA Solar Simulator (M/s Photo Emission Technology, USA).

Preparation of extract of natural dye sensitizers from bayberry (Myrica esculenta)

Methanol and hydrochloric acid were used as solvents for extracting bioactive compounds such as anthocyanins from the regional bayberry fruits of Uttarakhand. Fresh bayberries were washed with de-ionized water. After repeated washings, the pulp of the fruits was carefully separated from seeds and the pulp was manually mashed in a tub. The mashed pulp of the fruits was immersed in acidified methanol (HCl: methanol; 1:79 v/v) for 24 hours at room temperature and filtered to obtain the extract using Whatman filter paper no.1.

Fabrication of natural dye-sensitized solar cells

Preparation of photoanode

The FTO conductive side was dipped in ethanolic PLL solution for 1 hour. Titania nano powder synthesized by sol-gel method. The method is based on hydrolysing titanium tetraisopropoxide (TTIP) with acetic acid (4 M) and excess water (10 M). The solution was stirred by magnetic stirrer for 1 hour and then left for 24 hours at room temperature. After completion of 24 hours, a gel was obtained which was dried at 70 °C for 12 hours in an oven. Afterwards, it was dried at 100 °C to form TiO_2 crystals. The crystals were ground into a fine powder and then annealed at 300 °C and 500 °C to get the anatase phase.[60] The TiO_2 nano powder was then mixed with acetic acid and deionized water. A solution of α-terpineol in ethanol and ethyl cellulose in ethanol was prepared separately. The three solutions were mixed well to obtain a homogeneous paste. The TiO_2 paste was deposited on the FTO glass substrate surface using the doctor blade technique. The TiO_2 thin films were sintered on a vacuum setup (70 torr) at 80°C, 150 °C, 250 °C and 350 °C for 15 mins each, followed by final annealing at 500 °C for 1 hour. After cooling the TiO_2 thin films at room temperature, they were immersed in bayberry extract for 12 hours for

sensitization. We have used three different methods to fabricate TiO_2 films to evaluate the performance of solar cell and labelled them as **SLVA**, **DLVA** and **DLA**.

Method 1: Preparation of SLVA (Single-layered vacuum annealed): The FTO glass slide was dipped in PLL for 1 hour and dried at room temperature. A single layer of TiO_2 paste was then deposited onto the substrate using the doctor blade method. The coated film was subsequently subjected to stepwise sintering in a vacuum setup on a heating mantle at 80 °C, 150 °C, 250 °C and 350 °C for 15 mins each, followed by final sintering at 500 °C for 1 hour. After cooling to room temperature, the film, **SLVA,** was immersed in the dye extract for 12 hours.

Method 2: Preparation of DLVA (Double-layered vacuum annealed): The conducting side of the FTO glass was dipped in PLL for one hour and dried. A layer of TiO_2 paste was then applied onto the substrate using the doctor blade method, followed by vacuum treatment and stepwise sintering at 80 °C, 150 °C, 250 °C and 350 °C for 15 mins each. After cooling to room temperature, a second layer of TiO_2 paste was deposited using the same method and again subjected to identical vacuum treatment and stepwise sintering conditions of 80 °C, 150 °C, 250 °C and 350 °C for 15 mins each, followed by annealing at 500 °C for 1 hour. Finally, the film, **DLVA**, was cooled and immersed in the dye extract for 12 hours.

Method 3: Preparation of DLA (Double-layered annealed): The conducting side of the FTO glass slide was dipped in PLL for 1 hour and dried. A first layer of TiO_2 paste was then deposited onto the substrate using the doctor blade method. After drying the first layer at room temperature, a second layer of TiO_2 paste was applied over the first layer. The coated film was subsequently subjected to stepwise sintering at 80 °C, 150 °C, 250 °C and 350 °C for 15 mins

each, followed by final sintering at 500 °C for 30 min. After cooling to room temperature, the film, **DLA**, was immersed in dye extract for 12 hours.

Preparation of counter electrode

The counter electrode was fabricated using a 5 mM ethanolic solution of $H_2PtCl_6 \cdot 6H_2O$ deposited onto the conducting side of the FTO glass substrate with the help of drop casting method and heated at 350 °C for 15 minutes.

Preparation of electrolyte

Various working ratios of the two solutions viz. 0.5 M solution of potassium iodide in water and 0.05 M solution of iodine in acetonitrile were prepared and tested for DSSC applications under solar light. The results showed that the ratio of 0.7 ml of 0.5 M KI aqueous solution to 2.3 ml of 0.05 M I_2 solution in acetonitrile gave the best results.

Assembly of dye-sensitized solar cell

The photoanode and the counter electrode were sandwiched together using binder clips and electrolyte was introduced between them with the help of a dropper. Figure 10 illustrates the immobilization of natural dyes on TiO_2 surface of the photoanode of a DSSC.

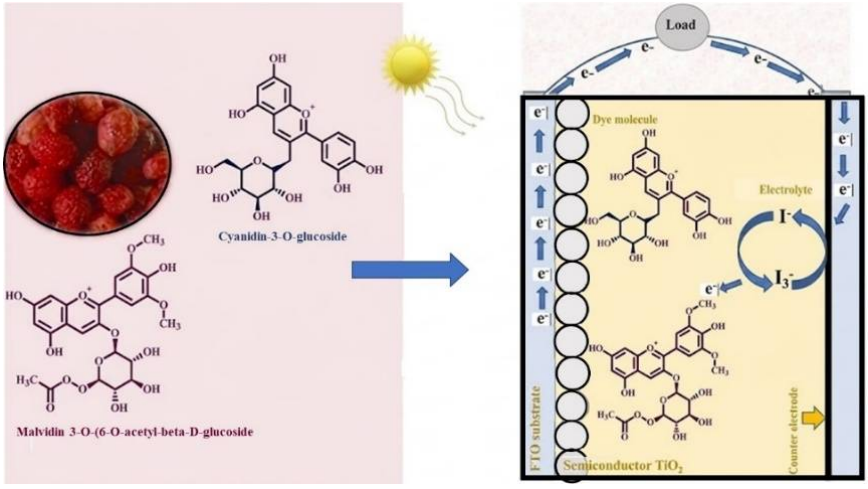

Figure 10. Immobilization of natural dyes on TiO_2 surface in a dye-sensitized solar cell.

Conclusions

Bayberry extract was successfully used as a natural photosensitizer in nanocrystalline TiO_2-based dye-sensitized solar cells (DSSCs). Characterization techniques such as high resolution-liquid chromatography mass spectrometry (HR-LCMS), UV-visible spectroscopy, fourier transform infrared spectroscopy (FTIR) and nuclear magnetic resonance spectroscopy (NMR) confirmed the presence of photosensitizing compounds, particularly anthocyanins, in the bayberry extract. The vacuum-annealed TiO_2 nanocrystalline layer was characterized by fourier transform infrared spectroscopy (FTIR), X-ray diffraction (XRD), scanning electron microscopy (SEM) and energy-dispersive X-ray spectroscopy (EDX), X-ray photoelectron spectroscopy (XPS) and non-contact atomic force microscopy (nc-AFM). The SLVA-based DSSC exhibited better conversion efficiency (0.32 %) than DLVA-based DSSC (0.09 %). Performance of DSSC fabricated from DLA-based DSSC showed the least conversion efficiency (0.06 %). The poor light harvesting from double-layered TiO_2 nanocrystalline films, **DLVA** and **DLA** showed that thickness of titania films affects the performance of DSSC. While DSSCs based on plant extracts rich in anthocyanin pigments have shown conversion efficiencies from 0.13 to 0.46 %, achieving higher performances entailed novel strategies. Yet, natural dye-based DSSCs have recorded much lower conversion efficiencies compared to silicon solar cells. Vacuum-annealing is known to introduce surface defects like oxygen vacancies that serve as effective coupling sites for energy states of organic dyes as well as defect states in TiO_2. The electron dynamics at the interface of the dye and TiO_2 determines the injection rate of electrons into the bulk of the semiconductor. If recombination effect of trapped electrons is much lower than electron injection rate in the semiconductor, then the performance of DSSC could enhance. The present work illustrates that controlled modification of photoanodes of a DSSC by vacuum-annealing the TiO_2 films offers a promising strategy for enhancing the photovoltaic performance of natural dye-

sensitized solar cells. The study demonstrates the potential of natural dyes extracted from bayberries to act as ecofriendly and low-cost sensitizers for photovoltaic applications. This work contributes to the development of environmentally safe and economically viable solar energy conversion devices.

Acknowledgements

The authors wish to thank to SAIF-IIT Bombay, IISER Bhopal, IIT Roorkee, IIT Indore and CSIR-National Physics Laboratory (New Delhi) for some characterization facilities. The authors also wish to acknowledge Department of Chemistry, H.N.B. Garhwal University, Srinagar-Garhwal, Uttarakhand for providing UV-visible spectroscopy facility.

Conflicts of interest

The authors have no competing interests to declare relevant to the content of this article.

References

1. Islam, M. M.; Biswas, M. T.; Nishat, S. M. Does renewable energy consumption lead to sustainable economic growth? Evidence from Bangladesh. *Int. J. Energy Water Resour*. **2026,** *10*, 53. https://doi.org/10.1007/s42108-026-00479-8
2. Dincer, I. Renewable energy and sustainable development. *Energy Sources* **2001,** *23*, 83 – 92. https://doi.org/10.1016/S1364-0321(99)00011-8
3. Bilgen, S.; Kaygusuz, K.; Sari, A. Renewable energy for a clean and sustainable future. *Energy Sources* **2004,** *26*, 1119 – 1127. https://doi.org/10.1080/00908310490441421
4. O'Regan, B.; Grätzel, M. A low-cost, high-efficiency solar cell based on dye-sensitized colloidal TiO_2 films. *Nature* **1991,** *353*, 737 – 740. https://doi.org/10.1038/353737a0
5. Nazeeruddin, M. K.; Baranoff, E.; Grätzel, M. Dye-sensitized solar cells: A brief overview. *Sol. Energy* **2011,** *85*, 1172 – 1178. https://doi.org/10.1016/j.solener.2011.01.018
6. Simkin, A. J., Kapoor, L.; Doss, C. G.; Hofmann, T. A.; Lawson, T; Ramamoorthy, S. The role of photosynthesis related pigments in light harvesting, photoprotection and enhancement of photosynthetic yield in planta. *Photosynth. Res.* **2022**, *152*, 23 – 42. https://doi.org/10.1007/s11120-021-00892-6

7. Maurya, I. C.; Neetu; Gupta, A. K.; Srivastava, P.; Bahadur, L. Progress in dye-sensitized solar cell materials. *J. Sol. Energy Eng.* **2016,** *138*, 051006. https://doi.org/10.1007/s11664-017-5759-3

8. Faiz, M. R.; Fahmi, A. Design considerations of DSSCs. *Int. J. Electr. Electron. Eng.* **2016,** *14*, 1 – 6.

9. Prabavathy, N.; Shalini, S.; Balasundaraprabhu, R.; Velauthapillai, D.; Prasanna, S.; Muthukumarasamy, N. Performance enhancement of DSSCs using natural dyes. *Int. J. EnergyRes.* **2017,** *41*, 1372 – 1383. https://doi.org/10.1002/er.3703

10. Narayan, M. R. Review of dye sensitized solar cells. *Renew. Sustain. Energy Rev.* **2012,** *16*, 208 – 215. https://doi.org/10.1016/j.rser.2011.07.148

11. Hug, H.; Bader, M.; Mair, P.; Glatzel, T. Biophotovoltaics: Natural dyes in solar cells. *Appl. Energy* **2014,** *115*, 216 – 225. https://doi.org/10.1016/j.apenergy.2013.10.055

12. Gaur, R. D. *Flora of District Garhwal North West Himalaya.* TransMedia: Srinagar (Garhwal), **1999**.

13. Mejica, G.F.C.: Ramaraj, R.; Unpaprom, Y. Natural dye (chlorophyll, anthocyanin, carotenoid, flavonoid) photosensitizer for dye-sensitized solar cell: A review. *Maejo Int. J. Energ. Environ. Comm.* **2022**, *4*(1), 12 – 22. https://doi.org/10.54279/mijeec.v4i1.247970

14. Devi, V. L.; De, D.; Kuchhal, P.; Pachauri, R. K. Photovoltaic Performance of TiO_2 and ZnO nanostructures in anthocyanin dye-sensitized solar cells. *Clean Energy* **2024**, *8*, 144 – 156. https://doi.org/10.1093/ce/zkae059

15. Maddah, H. A.; Berry, V.; Behura, S. K. Optimal design of spin-coated layers of TiO_2 for maximum open-circuit voltage in anthocyanin-based dye-sensitized solar cells. *Energy Convers. Manag*. **2025**, *346*, 120478. https://doi.org/10.1016/j.enconman.2025.120478

16. Salimian, J.; Osfouri, S.; Jalali, T. Synergistic effects of using the optimized anthocyanin extract from black plum (*Syzygium cumini*) and electrolyte concentration on the dye-sensitized solar cell photovoltaic performance. *J. Electron. Mater*. **2026**, *55*, 582 – 600. https://doi.org/10.1007/s11664-025-12530-1

17. Sampaio, D. M.; Babu, R. S.; Costa, H. R. M.; De Barros, A. L. F. Investigation of Nanostructured TiO_2 Thin Film Coatings for DSSCs Application Using Natural Dye Extracted from Jabuticaba Fruit as Photosensitizers. *Ionics* **2019**, *25*, 2893 – 2902. https://doi.org/10.1007/s11581-018-2780-5

18. Bekele, E. T.; Sintayehu, Y. D. Recent Progress, Advancements, and Efficiency Improvement Techniques of Natural Plant Pigment-Based Photosensitizers for Dye-Sensitized Solar Cells. *J. Nanomater*. **2022**, *1*, 1024100. https://doi.org/10.1155/2022/1024100

19. Dutta, A.; Gohain, B.; Trang, T. T.; Jennings, J. R.; Van Hao, N.; Konwer, S.; Gogoi, A.; Ekanayake, P. Application of natural photosensitizers in dye-sensitized solar cells: opportunities, challenges, and future outlook, *Photochem. Photobiol. Sci*. **2025**, *24*, 1443 – 1488. https://doi.org/10.1007/s43630-025-00762-3

20. Tsai, J. K.; Hsu, W. D.; Wu, T. C.; Meen, T. H.; Chong, W. J. Effect of Compressed TiO_2 nanoparticle thin film thickness on the performance of dye-sensitized solar cells. *Nanoscale Res. Lett.* **2013**, 8(1), 459. https://doi.org/10.1186/1556-276X-8-459

21. González-Verjan, V. A.; Trujillo-Navarrete, B.; Félix-Navarro, R. M.; de León, J. D.; Romo-Herrera, J. M.; Calva-Yáñez, J. C.; Reynoso-Soto, E. A. Effect of TiO_2 Particle and Pore Size on DSSC Efficiency. *Mater. Renew. Sustain. Energy* **2020**, *9*, 13. https://doi.org/10.1007/s40243-020-00173-7

22. Jabbar, H.; Abdullah, B. A.; Ahmad, N. Tuning TiO_2 Porosity of Multilayered Photoanode Towards Enhanced Performance of Dye Sensitized Solar Cell. *Al-Mustansiriyah J. Sci*. **2022**, *33*, 141 – 145. https://doi.org/10.23851/mjs.v33i4.1185

23. Duarte, A. E.; Cruz, A. L.; Marquina, A. V.; Martínez, J. A.; Juárez, A. G.; Islas, C. Z. One-step method to simultaneously grow TiO_2 compact and porous layers for DSSC photoelectrodes. *Appl. Nanosci.* **2024**, *14*, 819 – 826. https://doi.org/10.1007/s13204-023-03224-8

24. Kao, M. C.; Chen, K. H.; Hsiao, C. S. Effect of nanoparticle size on the photovoltaic performance of sol-gel-derived TiO_2 thin-film dye-sensitized solar cells. *Sens. Mater*. **2025**, *37*, 5071 – 5079. https://doi.org/10.18494/SAM5778

25. Pirdaus, N. A.; Ahmad, N.; Muhammad-Sukki, F.; Wan, W. A. A. Q. I. Effect of different titanium dioxide (TiO_2) deposition layers for dye-sensitized solar cell (DSSC) application. *Electrochim. Acta* **2025**, *527*, 146267. https://doi.org/10.1016/j.electacta.2025.146267

26. Obregón, S.; Rodríguez-González, V. Photocatalytic TiO_2 Thin Films and Coatings Prepared by Sol–Gel Processing: A Brief Review. *J. Sol-Gel Sci. Technol*. **2022**, *102*, 125 – 141. https://doi.org/10.1007/s10971-022-05778-3

27. Podelinska, A.; Neilande, E.; Pankratova, V.; Serga, V.; Bandarenka, H.; Burko, A.; Bocharov, D. V. Structural and spectroscopic characterization of TiO_2 nanocrystalline materials synthesized by different methods. *Nanomater*. **2025**, *15*, 498. https://doi.org/10.3390/nano15070498

28. Li, M.; Fang, Y.; Liu B. The effect of vacuum annealing on the structural, electric, and optical properties, and photocatalytic activities of sputtered TiO_2 and Nb-doped TiO_2 films. *Catalysts* **2025**, *15*, 166. https://doi.org/10.3390/catal15020166

29. Cui, Z.; Xu, Y.; Xu, Y.; Zhao, M.; Li, S.; Wang, J.; Pan, D.; Wu, W. Effects of solvent treatment on the formation of oxygen vacancy in TiO_2 via vacuum annealing. *J. Phys. Chem. C* **2022**, *126*, 21751 – 21758. https://doi.org/10.1021/acs.jpcc.2c06596

30. Gavrilin, I.; Dronov, A.; Volkov, R.; Savchuk, T.; Dronova, D.; Borgardt, N.; Pavlikov, A.; Gavrilov, S.; Gromov, D. Differences in the local structure and composition of anodic TiO_2 nanotubes annealed in vacuum and air. *Appl. Surf. Sci.* **2020**, *516*, 146120. https://doi.org/10.1016/j.apsusc.2020.146120

31. Li, Z.; Zhang, X.; Lu, G. Electron dynamics in dye-sensitized solar cells: Effects of surface terminations and defects. *J. Phys. Chem. B* **2010**, *114*, 17077 – 17083. https://doi.org/10.1021/jp108590f

32. Duncan, W. R.; Prezhdo, O.V., Theoretical studies of photoinduced electron transfer in dye-sensitized TiO_2. *Annu. Rev. Phys. Chem.* **2007**, *58*, 143 – 184. https://doi.org/10.1146/annurev.physchem.58.052306.144054

33. Dutta, A.; Gohain, B.; Trang, T. T.; Jennings, J. R.; Van Hao, N.; Konwer, S.; Gogoi, A.; Ekanayake, P. Application of natural photosensitizers in dye-sensitized solar cells: opportunities, challenges, and future outlook. *Photochem. Photobiol. Sci*. **2025**, *24*(8), 1443 – 1488. https://doi.org/10.1007/s43630-025-00762-3

34. Nautiyal, S.; Semwal, D.K.; Semwal, R. B. Assessment of traditional knowledge on dye-yielding plants in the Jaunpur region of the Uttarakhand Himalayas. *Vegetos* **2025**, 1 – 10. https://doi.org/10.1007/s42535-025-01330-x

35. Bhandari, N. L.; Pokhrel, B.; Bhandari, U.; Bhattarai, S.; Devkota, A.; Bhandari, G. An overview of research on plant based natural dyes in Nepal: scope and challenges. *J. Agric. Nat. Res*. **2020** *3*, 45 – 66. https://doi.org/10.3126/janr.v3i2.32328

36. Mohammad, F. Natural colorants in the presence of anchors so-called mordants as promising coloring and antimicrobial agents for textile materials. *ACS Sustainable Chem. Eng*. **2015**, *3*, 2361 – 2375. https://doi.org/10.1021/acssuschemeng.5b00537

37. Smitha, C. K.; Ramachandran, A.; Athira, K. K. Green Synthesis of nanoparticles: A comprehensive review of key parameters, characterization methods, and applications; In Green Nanotechnology: Innovations and Applications in Biofuels, Environmental Management and Healthcare. Nanotechnology in Plant Sciences; Geetha, N.; Arunachalam, K. (eds); Springer, Cham. **2026**, *5*, 399 – 445. https://doi.org/10.1007/978-3-032-17170-2_17

38. Kabra, A.; Sharma, R.; Hano, C.; Kabra, R.; Martins, N.; Baghel, U. S. Phytochemical composition, antioxidant, and antimicrobial attributes of different solvent extracts from myrica esculenta buch.-ham. Ex. D. Don leaves. *Biomolecules* **2019**, *9*, 357. https://doi.org/10.3390/biom9080357

39. Supriyanto, E.; Kartikasari, H. A.; Rohman, L.; Alviati, N.; Sutjipto, A. G. E. Estimate dye sensitized solar cells performance using dyes based on green-future and local wisdom with simulation method. *Mater. Sci. Forum* **2020**, *981*, 92 – 97. https://doi.org/10.4028/www.scientific.net/MSF.981.92

40. AL-Mojahid, F. Q.; Cherian, T.; Alsosowaa, A. A.; Devi, N. S.; Ardra, A. P.; Vijay, N.; Asokan, S.; Merlin, T.; Peijnenburg, W. J. phytochemical profile, antioxidant, antimicrobial activity, antibiofilm, cytotoxicity, and HR-LCMS of *Tribulus terrestris*. *J. Genet. Eng. Biotechnol*. **2026**, *24*, 100683. https://doi.org/10.1016/j.jgeb.2026.100683

41. Pawar, D. S.; Nasreen, S. HR-LCMS of phytoconstituents and antifungal activity of medicinal plants. *J. Med. Plants Stud.* **2018**, *6*, 173 – 176.

42. Bhattacharya, A.; Chattopadhyay, R. R. Isolation, identification and chemical characterization of compounds from phenolic extracts of peels of kufri chipsona-3 and kufri jyoti potatoes having synergistic antioxidant interactions in combination. *J. Food Nutr. Diet Sci.* **2024**, 29 – 40. https://doi.org/10.55976/fnds.22024123129-40

43. Sasikumar, R.; Vivek, K.; Panda, S. K.; Jaiswal, A. K. Formulation and characterization of ready-to-drink nutraceutical beverage from blood fruit (*Haematocarpus validus*). *LWT* **2025**, *225*, 117929. https://doi.org/10.1016/j.lwt.2025.117929

44. Noumi, E.; Snoussi, M.; Anouar, E. H.; Alreshidi, M.; Veettil, V. N.; Elkahoui, S.; Adnan, M.; Patel, M.; Kadri, A.; Aouadi, K.; De Feo, V. hr-lcms-based metabolite profiling, antioxidant, and anticancer properties of *Teucrium polium L.* methanolic extract: computational and *in vitro* study. *Antioxidants* **2020**, *9*, 1089. https://doi.org/10.3390/antiox9111089

45. Neupane, P.; Lamichhane, J. Phytochemical Profiling Using HRLCMS and Evaluation of Antioxidant and Antibacterial Activities of Nepalese Medicinal Plants. *Vegetos* **2020**, *33*, 628 – 640. https://doi.org/10.1007/s42535-020-00143-4

46. Parsaila, N.; Navale, A. M.; Shelke, A. B.; Patidar, N.; Sharma, D.; Shinde, S.; Mishra, B.; Singh, S. M.; Soni, J. Protective effect of aqueous extract of *Myrica Esculenta* against cyclophosphamide-induced spermatogenesis dysfunction in

Wistar rats via antioxidant Signaling pathway. *Toxicol. Res*. **2025**, *14*, tfaf173. https://doi.org/10.1093/toxres/tfaf173

47. Havsteen, B. H. The biochemistry and medical significance of flavonoids. *Pharmacol. Ther.* **2002**, *96*, 67 – 202. https://doi.org/10.1016/S0163-7258(02)00298-X

48. Saha, S.; Singh, J.; Paul, A.; Sarkar, R.; Khan, Z.; Banerjee, K. Anthocyanin extraction and characterization. *J. AOAC Int.* **2020,** *103*, 23 – 30. https://doi.org/10.5740/jaoacint.19-0201

49. Sutharut, J.; Sudarat, J. Total anthocyanin content and antioxidant activity. *Int. Food Res. J.* **2012,** *19*, 215 – 221.

50. Ahliha, A. H.; Nurosyid, F.; Supriyanto, A.; Kusumaningsih, T. Fabrication of DSSCs using natural dyes. *IOP Conf. Ser.: Mater. Sci. Eng.* **2018,** *333*, 012018. https://doi.org/10.1088/1757-899X/333/1/012018

51. Ramamoorthy, R.; Radha, N.; Maheswari, G.; Anandan, S.; Manoharan, S.; Williams, R. V. Electrochemical properties of TiO_2 films. *J. Appl. Electrochem.* **2016,** *46*, 929 – 937. https://doi.org/10.1007/s10800-016-0974-9

52. Fernandes, A.; Brás, N. F.; Mateus, N.; De Freitas, V. Anthocyanin stability and reactivity: relevance to performance as food colorants. *New J. Chem.* **2015**, *39*, 2602 – 2611. https://doi.org/10.1039/C4NJ02339K

53. Thamaphat, K.; Limsuwan, P.; Ngotawornchai, B. Phase characterization of TiO_2 powder by XRD and TEM. *Agric. Nat. Resour.* **2008,** *42*, 357 – 361. http://creativecommons.org/licenses/by-nc-nd/4.0/

54. Sta, I.; Jlassi, M.; Hajji, M.; Boujmil, M. F.; Jerbi, R.; Kandyla, M.; Kompitsas, M; Ezzaouia, H. Structural and optical properties of TiO_2 thin films prepared by spin coating. *J. Sol-Gel Sci. Technol.* **2014,** *72*(2), 421 – 427. https://doi.org/10.1007/s10971-014-3452-z

55. Sankapal, B. R.; Lux-Steiner, M. C.; Ennaoui, A. TiO_2 thin films for photovoltaic applications. *Appl. Surf. Sci.* **2005,** *239*, 165 – 170. https://doi.org/10.1016/j.apsusc.2004.05.142

56. Perillo, P. M.; Rodriguez, D. F. Influence of the anatase/rutile phase ratio on the photoresponse of TiO_2 thin films. *J. Solid State Electrochem.* **2026**, *30*, 1233 – 1241. https://doi.org/10.1007/s10008-025-06466-z

57. Bakri, A. S.; Sahdan, M. Z.; Adriyanto, F.; Raship, N. A.; Said, N. D. M.; Abdullah, S. A.; Rahim, M. S. Effect of annealing temperature of titanium dioxide thin films on structural and electrical properties. *AIP Conf. Proc.* **2017**, *1788*, 030030. https://doi.org/10.1063/1.4968283

58. Vasu, R.; V. T. A. S. Tailoring TiO_2 thin film properties through spin-coating and rotational speed effects. *Braz. J. Phys.* **2026,** *56*, 78 – 85. https://doi.org/10.1007/s13538-025-01967-8

59. Cui, Z.; Zhao, M.; Que, X.; Wang, J.; Xu, Y.; Ghazzal, M. N.; Wu, W. Vacuum annealing-induced modification of TiO_2 for enhanced photocatalysis. *ACS Omega* **2021,** *6*, 27121 – 27128. https://doi.org/10.1021/acsomega.1c03762

60. Behnajady, M.A.; Eskandarloo, H.; Modirshahla, N.; Shokri, M. Sol-gel low-temperature synthesis of stable anatase-type TiO_2 nanoparticles under different conditions and its photocatalytic activity. *Photochem. Photobiol.* **2011**, *87*, 1002 – 1008. https://doi.org/10.1111/j.1751-1097.2011.00954.x